

Arbitrary control of the temporal waveform of photons during spontaneous emission

Carl Thomas*, Rebecca Munk, and Boris Blinov

*Department of Physics, University of Washington**

(Dated: December 1, 2025)

Control of the temporal waveform and Fock state statistics of photons produced during spontaneous emission from single quantum emitters provides a crucial tool in the establishment of hybrid quantum systems, optimal state transfer and interferometric stability of network architectures based on flying qubits. We describe a method to generate photons of any temporal waveform from emitters of any lifetime. Our broadly applicable approach has only two requirements for a candidate qudit: (1) control of the phase-parity and (2) modulation of the amplitude of a field coupling a ground state to an excited manifold which produces a photon during relaxation. We detail how to find optimal excitation pulse shapes, both numerically and experimentally, by employing variational algorithms to feedback on atomic populations. Additionally, we develop Quantum Monte Carlo based tools to determine emission statistics and establish techniques for optimal post-selection to ensure maximum fidelity of photon generation protocols. We situate our work in the context of other prior research on bespoke single photon sources and networking including post-emission pulse shaping, temporal gating and cavity-based methods. In comparison, our free-space process has greater flexibility in producing any waveform, requires less infrastructure and can be readily applied across a wide domain of emitters of any frequency or lifetime. We demonstrate temporal waveform shaping in $^{174}\text{Yb}^+$ trapped ions. Using feedforward validation of photon waveforms, we estimate an achievable process fidelity of at least ≈ 0.996 .

I. INTRODUCTION

The ability to control the state of single photons produced during spontaneous emission represents a key tool for building quantum networks and enabling mixed-architecture qubit platforms. For example, the production of indistinguishable photons from distinct qubit implementations would allow the application of established entanglement generation protocols to be used to realize hybrid quantum systems [1, 2]. Such systems could leverage the strengths of various qubit types such as the long coherence times of ions or the fast gate speeds of solid state spin donors to out compete any single-qubit type platform [3].

Building photon-mediated hybrid systems requires control over the state of a flying qubit in all bases including frequency, polarization, number, spatial mode and time bin [4]. This work deals with both arbitrary control of temporal waveform of photons produced by network nodes as well as methods to model and mitigate the effects of multiple excitations from a single node which can degrade photon based network protocols.

A. Photon temporal waveform control

Advances in quantum frequency conversion provide a promising avenue to bridge large spectral mismatch between emitters [5, 6]. Photon polarization can be controlled via mapping dipole emission fields to lab-frame field orientations [7]. Meanwhile, spatial mode control

can be achieved via the use of cavities [8, 9], fiber based waveguides [10] or simple masking techniques [11] while spatial light modulators present reconfigurability and flexibility for a range of protocols [12].

In tandem with these techniques, control over the photon temporal waveform would allow any two quantum emitters to generate identical photons. By matching the photon emission probabilities of both nodes, various single [4, 13, 14] and two [15] photon detection methods, well established in same type qubit networks, could be used to entangle mixed-architecture quantum systems. Photon based remote entanglement techniques have been independently implemented in neutral atoms [16], solid state systems [17] and trapped ions [18]. However, to date, no such protocol has been demonstrated between *distinct* qubit platforms. Previously, interference of photons from a trapped ion and (telecom converted) neutral atom ensemble has been achieved; however, photon mixing relied on temporal gating to ensure high contrast [19]. The efficiency of gating based approaches decreases as the mismatch of excited state lifetimes grows, making it is desirable to find an alternative approach for ensuring high similarity between emitted photons.

Full control of the temporal envelope of single photons would also allow optimization of processes such as quantum state transfer in repeater protocols. By matching the time-reversed natural decay shape of an atomic line, the probability that a photon emitted by one node in a network will be absorbed by a subsequent node can be maximized [20, 21]. Similarly, in atom-cavity systems, tailoring photon shapes to impedance match an optical resonator can be used to enhance flying-stationary qubit coupling [22].

Same qubit type networks can also benefit from task specific tailored single photons in other ways. In trapped

* cjthoma@uw.edu

ion photonic interconnects, for example, photons from distributed traps are most often produced via strong, short excitation pulses [23, 24]. In such systems, the resultant photon waveform closely matches the Fourier transform-limited Lorentzian line-shapes of the excited state, yielding a temporal distribution with an exponentially decaying tail with the damping rate determined by the state lifetime. While photons from two such nodes will interfere perfectly assuming no timing or interferometric error sources, the fidelity of remote entanglement operations for such experiments may be degraded by non-common mode path fluctuations of each arm of the photon detection apparatus [4]. The deleterious effects of path dependent phase fluctuation can be minimized by appropriate selection of photon distributions with gaussian waveforms being the most robust to path length instability [25].

Timing jitter of excitation pulses may lead to similar effects. For instance, considering a ‘typical’ ion-ion remote entanglement scheme, a set of synchronized excitation pulses for each node may be controlled by independent arbitrary waveform generators (AWG) sharing a common clock. For a commercially available AWG common in research labs, the jitter which parameterizes timing offset between a trigger pulse and output waveform is often on the order of 150 ps. To gain a sense for the how such an error will affect the photon indistinguishability, defined as the mode overlap, from two nodes, we can consider a photon interference protocol wherein two qubit nodes are subjected to instantaneous excitation pulses separated by 150 ps. In the case where the excited state life time of each node is ≈ 8 ns, common in many popular ionic qubits, the resultant photon indistinguishability will be 0.963. However, when excitation is driven such that the photons have distributions described by a gaussian with a full-width-half-max of 15 ns, this increases to 0.9997. This corresponds to a reduction in photon indistinguishability error by more than a factor of 10^2 . As such, the ability to produce photons of arbitrary temporal shape could prove useful in future long distance distributed quantum systems.

In addition to temporal gating of photon detection times, alternative approaches to the control of photon temporal waveform have made use of post-emission tools such as circuit based pulse shaping via dispersive optics [26], electro-optical modulation of photon wave packets [27–29] or measurement based post selection techniques [30]. However, such methods are not widely applicable across all frequency bands owing to hardware limitations. Additionally, post-emission shaping may introduce additional noise or loss into the system.

Approaches which aim to control photon waveform in-situ (ie. during the emission process rather than post hoc) by embedding the emitter in a cavity have been widely implemented or proposed in many qubit platforms including ions [31], quantum dots [32] and neutral atoms [33]. Cavity-based Stimulated Raman Adiabatic Passage (STIRAP) experiments modulate driving fields to

control photon shape during emission. These STIRAP techniques allow the deterministic emission of photons of arbitrary distributions within certain constraints. For instance, the adiabatic condition and cavity properties limit the minimum scale of temporal features in the resultant photons. Additionally, such approaches require specialized optics and are necessarily coupled to the resonator modes [34–36]. The use of a cavity also leads to practical challenges for scaling due to the need for additional infrastructure in already crowded qubit platforms. Moreover, while emission into a cavity mode is advantageous for some networking tasks, it can be less suitable for protocols that encode atom-photon entanglement in multiple orthogonal modes (e.g. polarization or frequency two-photon schemes), unless the resonator is explicitly engineered to support multiple qubit emission paths [37].

The technique we demonstrate makes use of a free space quantum emitter wherein shaping of the photon temporal waveform is realized by deterministic modulation of the population of the state undergoing radiative decay. This control is realized by combining optimization of the pulse envelope with parity phase control for a field which couples a ground and excited state. The conceptual approach and numerical methods to identify optimal excitation pulses for this approach are discussed in Sec. II. Experimental realization is addressed in Sec. IV.

B. Mitigating multi-photon emission events

In addition to control of the temporal profile of photons produced during excitation events, network protocols must also address the contributions of multiple photon excitations from a single node. Finite-duration excitation pulses inevitably introduce a nonzero probability of multiple photon emissions during a single entanglement attempt. In weak-excitation single-photon schemes of the Cabrillo type [38], the heralding signal is associated with a single photon emission. Any additional emission leaves which-path information in the environment and reduces the fidelity of the heralded remote Bell state. In practice, when the excitation pulse length is comparable to the excited-state lifetime, a photon emitted early in the pulse can be followed by re-excitation and a second emission within the same trial, even if the total emission probability is kept small.

These effects are generic across architectures based on spontaneous emission. Analyses of remote entanglement schemes explicitly show that multi-photon events set a trade-off between entanglement generation rate and fidelity: increasing the emission probability raises the heralding rate but also enhances the weight of higher-order photon-number components and thus degrades the quality of the entangled state [39–41]. It is therefore essential to (i) model the full photon-number statistics associated with a given temporal pulse shape, (ii) operate in regimes where the multi-photon probability is

quantitatively controlled, and (iii) design temporal post-selection strategies that suppress contributions from trajectories involving more than one emission event. These considerations motivate the Quantum Monte Carlo based tools developed in Sec. III, which we use to characterize and mitigate multi-photon error channels for shaped waveforms. These same techniques also provide the basis to perform post-selection, allowing improved photon interference.

II. ANY EMITTER, ANY PHOTON TEMPORAL WAVEFORM

We describe the process to find the optimal form of the coupling field to generate photons of a desired temporal shape for the instance of a $^{174}\text{Yb}^+$ ion. By adapting the Hamiltonian describing the time evolution of the system, this approach can be applied to higher dimensional Hilbert spaces corresponding to more general multi-level qudits. As we consider excitation processes which drive the $(^2\text{S}_{1/2}, m_J = -1/2) \equiv |0\rangle \Rightarrow (^2\text{P}_{1/2}, m_J = +1/2) \equiv |1\rangle$ transition and collect π photon emitted as the state relaxes to $(^2\text{S}_{1/2}, m_J = +1/2) \equiv |2\rangle$, we need only model a 3-level Λ system. Experimentally relevant atomic levels are shown in Fig. 1. Both the numerical and experimental realizations of the photon shaping process follow the same basic ‘recipe’ described below.

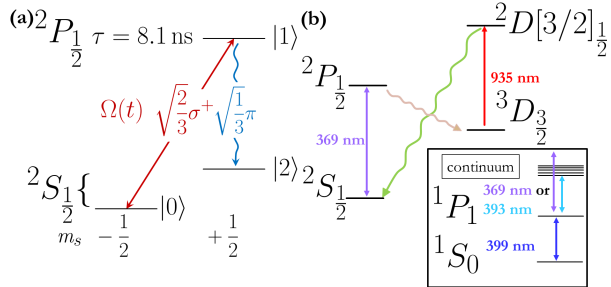


FIG. 1. Partial level structure of $^{174}\text{Yb}^+$ relevant for photon control experiments. (a) Optical pumping to $|0\rangle$ via the application of σ^- polarized light (not shown) initializes the system. The application of a time-dependent complex Rabi frequency, $\Omega(t)$, drives the transition from $|0\rangle$ to $|1\rangle$ to control the excited state population, $\rho_{11}(t)$. Spontaneous emission from $|1\rangle$ generates photons with a temporal waveform at rate $\Gamma \times \rho_{11}(t)$ in a superposition of σ^+ and π polarizations with a relative amplitude of 2:1. (b) Expanded atomic level system showing relevant laser frequency for photo-ionization and repumping.

A. Photon shaping recipe

Our basic approach to produce a photon of a desired temporal waveform is as follows:

1. Initialize the system in the $|0\rangle$ state. Experimentally, this is achieved by the application of circu-

larly polarized light with a \mathbf{k} -vector perpendicular to the quantization axis.

2. Define an interaction Hamiltonian which represents a σ^+ driving field coupling $|0\rangle$ to $|1\rangle$. Experimentally, this represents a temporally shaped, resonant, and circularly polarized laser pulse of the opposite handedness used to perform optical pumping. In order to simulate realistic parameters, we restrict the maximum Rabi frequency to 250 MHz based on standard available laser power and optics for typical dipole transitions in ion trapping.
3. Solve the system time-evolution to find $\rho_{11}(t)$. As $|1\rangle$ undergoes spontaneous emission, the temporal distribution of the resulting photon follows the excited state population. This process is described by solving the Lindblad master equation. Numerically, this is achieved by modeling the system using Qutip. Experimentally, the laser pulse is applied and the resultant time of detection of the photon is recorded. The state is then reinitialized in $|0\rangle$ and the process is repeated until a sufficiently dense photon histogram can be constructed.
4. Once the form of the emitted photon is determined, iteratively update H_{int} , or equivalently, the laser pulse shape, utilizing a variational algorithm until the predicted or measured photon shape converges with the desired distribution.

Depending on the application of photon shaping, particular details of wavefunction optimization will vary; however, the basic approaches and considerations described throughout this and subsequent sections continue to apply. For example, in our remote entanglement application, we describe photons optimized specifically for single-photon remote entanglement schemes well established in the literature [42]. In such experiments, two remote matter qubits undergo weak, synchronized, pulsed excitation in order to produce identical photons with low single photon emission probabilities. These photons are then combined on a beam splitter and counted with number resolving detectors such that a single photon measurement projects the joint matter qubit system into a Bell state. As such, we aim to optimize the temporal wave packet of photons corresponding only to π emission and trace out the contribution of σ^+ events. However, for applications such as the standard 2-photon polarization based remote entanglement schemes commonly employed in trapped ions [43], the entire photon temporal wavefunction corresponding to both π and σ^+ must be considered. For such an experiment, the same basic approach to waveform optimization can be employed with the only differences being the need to track the temporal waveforms of both polarization paths and different merit functions for photon emission statistics.

B. Quantum optics of photon generation

In this subsection, we present the relevant physics to model the photonic waveform produced via spontaneous emission during the atom-light interaction. The laser is modeled as time-dependent field which couples states $|0\rangle$ and $|1\rangle$, driving the transition with Rabi frequency $\Omega(t)$. We additionally allow the laser to be modulated by a time dependent phase which will become relevant for coherent de-excitation. For a Λ system driven by a laser with envelope $\Omega(t)$, frequency ω_L and controllable phase offset $\phi(t)$, after applying the rotating wave approximation, we can write the interaction Hamiltonian as

$$H_I = \frac{\hbar}{2} \Omega(t) (e^{i(\omega_L t + \phi(t))} |0\rangle\langle 1| + e^{-i(\omega_L t + \phi(t))} |1\rangle\langle 0|). \quad (1)$$

The atomic Hamiltonian simply captures the splitting between the excited state and ground states (initially assuming degenerate S Zeeman levels),

$$H_0 = \hbar\omega_0 |1\rangle\langle 1|. \quad (2)$$

Thus, in matrix form, we have $H_{\text{total}} = H_I + H_0$ which can be explicitly written as

$$H = \frac{\hbar}{2} \begin{pmatrix} 0 & e^{i(\omega_L t + \phi(t))}\Omega(t) & 0 \\ e^{-i(\omega_L t + \phi(t))}\Omega(t) & 2\omega_0 & 0 \\ 0 & 0 & 0 \end{pmatrix}. \quad (3)$$

Adopting a frame which rotates at frequency ω_L , we can include terms for time dependent laser detuning, given by $\Delta(t) = \omega_L(t) - \omega_0$ and any ground state splitting, δ . This yields

$$\tilde{H}(t) = \frac{\hbar}{2} \begin{pmatrix} 0 & \Omega(t) e^{+i\phi(t)} & 0 \\ \Omega(t) e^{-i\phi(t)} & -2[\Delta(t) + \dot{\phi}(t)] & 0 \\ 0 & 0 & 2\delta \end{pmatrix}. \quad (4)$$

The addition of the $e^{\pm i\phi(t)}$ terms accounts for relative phase between the atomic states and local oscillator (i.e. laser). As we will only ultimately control the phase-parity of the laser, this means that $\phi(t)$ will always either be 0 or π . In other words, the $H_{0,1}$ and $H_{1,0}$ matrix elements will be allowed to switch sign. Intuitively, we see that the addition of a π phase will reverse the direction of population transfer between $|0\rangle$ and $|1\rangle$.

Spontaneous emission occurs from $|1\rangle$ along two paths via production of a σ^+ or π polarized photon. The excited state scatters photons at a rate given by $\Gamma = 1/\tau \approx 123$ MHz. We introduce collapse operators $L_1 = \sqrt{\Gamma_{\sigma^+}} |0\rangle\langle 1|$ and $L_2 = \sqrt{\Gamma_\pi} |2\rangle\langle 1|$ where the relative amplitude between σ^+ and π is 2:1, determined by the corresponding Clebsch-Gordon coefficients for each decay path such that $\Gamma = \Gamma_{\sigma^+} + \Gamma_\pi$.

The Lindblad master equation for the atom can then be written as

$$\frac{d\rho}{dt} = -\frac{i}{\hbar} [H, \rho] + \sum_{k \in \{\pi, \sigma^+\}} (L_k \rho L_k^\dagger - \frac{1}{2} \{L_k^\dagger L_k, \rho\}) \quad (5)$$

with $|\psi_0\rangle_{\text{atom}} = |0\rangle$. We employ numerical methods to solve the master equation for a given form of $\Omega(t)$ to determine the corresponding value of $\rho_{11}(t)$ from which the temporal profiles of both σ^+ and π photons are derived.

If we consider an excitation pulse of finite duration, we can describe the relative temporal flux, $I(t)$, of photons emitted into polarization mode $q \in \{\pi, \sigma^+\}$ as

$$I_q(t) \propto \Gamma_q \rho_{11}(t), \quad \sum_q \Gamma_q = \Gamma. \quad (6)$$

Normalizing $I_q(t)$ yields the temporal intensity envelope of the photons emitted during this process

$$|g_q(t)|^2 = \frac{\Gamma_q \rho_{11}(t)}{\langle N_q \rangle}, \quad \int |g_q(t)|^2 dt = 1. \quad (7)$$

Here, $\langle N_q \rangle$ is the mean photon emission number into polarization mode q given by:

$$\langle N_q \rangle \equiv \int_{t_0}^{t_f} \Gamma_q \rho_{11}(t) dt. \quad (8)$$

For the case of single emissions, we can write the state of the resultant photons using polarization-time mode creation operators,

$$|1_{g_q}^{(q)}\rangle = \int dt g_q(t) \hat{a}_q^\dagger(t) |vac\rangle, \quad \int dt |g_q(t)|^2 = 1. \quad (9)$$

Because the emission of a π photon projects the electron into a dark state (i.e. σ^+ polarized light cannot excite a photon from $|2\rangle$), we have the condition $\langle N_\pi \rangle \leq 1$. As the atom can produce at most one π photon, we have a two dimensional subspace spanned by $\{|vac\rangle, |1_{g_\pi}^{(\pi)}\rangle\}$ with $P_0 = 1 - \langle N_\pi \rangle$ and $P_1 = \langle N_\pi \rangle$ respectively. The same approach could be used to characterize the mean photon emission number for σ decay. However, since the emission of a σ polarized photon projects the atom back into $|0\rangle$, re-excitations are possible and the final inequality does not hold. In practice, it is usually sufficient to curtail this basis to just a few polarization-time basis states depending on the strength and duration of the pulse.

For the low excitation regime, we can often neglect any amplitude of multiple emissions caused by re-excitation following a σ path decay. Setting $\delta = 0$ such that Zeeman levels are degenerate, we can write the entangled atom-photon state as

$$|\Psi\rangle = \sqrt{1 - \langle N \rangle} |0_A\rangle |vac\rangle + \sqrt{\langle N_\sigma \rangle} |0_A\rangle |1_{g_\sigma}^\sigma\rangle + \sqrt{\langle N_\pi \rangle} |2_A\rangle |1_{g_\pi}^\pi\rangle, \quad (10)$$

where $\langle N \rangle = \langle N_\pi \rangle + \langle N_\sigma \rangle$.

In principle, one can always write the full atom-field state as a pure state in a joint Hilbert space. However, once we allow for the possibility of multiple emissions, even in the restricted case where at most a single π photon can be produced while any number of σ photons may

be scattered, the pure state becomes a superposition over many different photon polarization-temporal modes and emission histories. The atom may emit zero, one, two, or more σ photons at different times before a terminating π emission (or no π emission at all), and each such sequence of jumps leaves the atom in a different correlated state $|\chi_{n_\sigma, n_\pi}\rangle_A$ with $(n_\sigma, n_\pi) \in \{0, 1, 2, \dots\} \times \{0, 1\}$. The exact pure state is therefore a highly entangled sum over all allowed (n_σ, n_π) , with amplitudes that depend on the full time record of the jumps, and cannot be expressed solely in terms of the mean photon numbers $\langle N_\sigma \rangle$ and $\langle N_\pi \rangle$.

Identifying excitation pulses wherein the ‘at most one photon’ approximation provides an accurate estimate of the actual state of the atom-photon system is a non-trivial problem. How closely the state given by the low emission approximation matches the true atom-photon wavefunction depends not only on $\langle N \rangle$, but also on the temporal distribution of emitted photons. Importantly, we cannot determine the relative probabilities of n -photon events or temporal correlations between photon emission times using $\langle N \rangle$ alone. For instance, even in the case where $\langle N \rangle$ is small (say 0.2), there will still be some probability for any such excitation process that 2, 3 or more photons were emitted. Additionally, when multiple photons are emitted, they will occupy distinct temporal modes due to antibunching which cannot be directly predicted by simply determining $\rho_{11}(t)$. We will return to this problem in Sec. III.

C. Numerical results for photon temporal waveform control

Through numerical exploration, we find that an appropriate form of the interaction Hamiltonian can be determined to produce photons of any relative temporal distribution. However, it is important to note that for a target photon shape it is not generally possible to simultaneously control the Fock state basis of the desired polarization-temporal waveform. If both the relative shape and associated emission probability are considered, limits on achievable state preparation fidelity depend on intrinsic properties of the emitter used to generate photons and target distribution. An upper bound on achievable values of $\langle N \rangle$ for a desired photon distribution, $g(t)$, is provided in Appendix A.

To contextualize the results of the numerical photon waveform optimization, we divide target distributions into four representative classes based on the limits described in the aforementioned appendix. They are as follows:

- Natural photons:** this is the photon generated by an excitation pulse of infinitely short duration. This yields a temporal distribution following an exponential decay set by the excited state lifetime. These are referred to as ‘natural’ as this is the photon shape determined purely by the excited state

line shape.

- Long photons:** these are smooth monotonic photons with temporal spreads larger than natural photons.
- Short photons:** these are smooth monotonic photons with temporal spreads smaller than natural photons.
- Weird photons:** these are photons whose temporal distributions include discontinuities or are non-monotonic.

In order to arrive at ideal forms of the interaction Hamiltonian to produce a desired photon distribution, we employed one of several optimization algorithms. Initial attempts at waveform optimization relied solely on control of the instantaneous Rabi frequency amplitude to optimize predicted photon distributions. Numerical results demonstrate that pulse amplitude modulation is sufficient to produce long photons of any $\langle N \rangle$ with arbitrarily high fidelities. However, we found that as target photon distributions are made shorter and shorter vis-à-vis the state lifetime, the ‘amplitude modulation only’ approach fails. In other words, we cannot generate short or weird photons with high fidelities by control of $|\Omega(t)|$ alone. The reasons for these limitations are threefold:

- The contribution of spontaneous emission to $|0\rangle$ at times early in the excitation process leads to some amplitude of incoherent re-excitation. This error grows with $\langle N \rangle$ and is minimized for emitters with a small $|0\rangle : |2\rangle$ branching ratio. This contribution is also minimized for small ratios of photon width to excited state lifetime, τ , as such distributions suppress the probability of multi-photon events.
- Intrinsic dephasing time between $|0\rangle \rightarrow |1\rangle$ limited, in the absence of any environmental noise, by the relaxation rate of the excited state can alternatively be understood as a loss of coherence between the qudit transition and the driving field leading to an inability to coherently control the excited state population. This also leads to a contribution of incoherent excitation with an amplitude which grows with $\langle N \rangle$.
- Decay dynamics cannot be inverted without a coherent π pulse of unphysically short duration preventing turning points or discontinuities in $P_1(t)$.

For a given atomic system, points (1) and (2) are unavoidable and result from the fundamental characteristic of the transition employed in photon shaping. The magnitude of their contributions to infidelity in photon generation depend highly on the transition chosen, the desired photon shape and target $\langle N \rangle$. These effects can be seen by increasing the target value of $\langle N \rangle$ for a single, normalized target photon waveform generated by the same emitter in each case as reflected in Fig. 2.

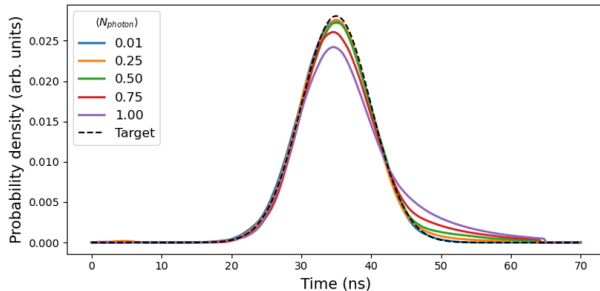


FIG. 2. The best possible photon temporal waveforms which can be produced by a single emitter as target $\langle N \rangle$ is increased. Incoherent re-excitation leads to greater weight in photon tail at later times. These effects are suppressed in long photon temporal distributions.

However, as both effects result from the intrinsic dephasing resulting from spontaneous emission, their contributions to total infidelity can be limited by operating in a low $\langle N \rangle$ regime if a decrease in photon generation rate can be tolerated.

While the generation of long photons proves suitable for many applications, ideally we would like to have the ability to produce photons of any temporal distribution, regardless of the lifetime of the emitter used. Our technique to generate short and weird photons relies on an additional degree of freedom in the interaction Hamiltonian describing excitation, beyond simply modulating the instantaneous Rabi frequency. We introduce the additional flexibility of modulating the relative phase of the driving field over the course of a single excitation pulse. Experimentally, this amounts to advancing or delaying the wavefront of the excitation laser pulse by an (ideally) instantaneous fixed phase during a single shot. While this approach does not allow for the production of photons of both an arbitrary $g(t)$ and $\langle N \rangle$, we find that in tandem with amplitude modulation, bit-wise control of the relative phase of the excitation laser should permit the production of photons of any relative temporal waveform.

We motivate this approach by analogy to the interaction between a light field and a Fabry-Perot resonator wherein a resonant optical wave packet excites a single cavity mode with light leaking out of the cavity at a rate determined by the resonator quality factor. By advancing the phase of the laser by π part way through the pulse duration, the mode field amplitude can be reduced to 0 at a rate faster than would otherwise be possible. In the rotating frame, a step $\phi \rightarrow \phi + \pi$ is equivalent to switching the sign of the Rabi frequency. A negative Rabi frequency pumps population out of the excited state through stimulated emission.

The phase modulation technique can also be understood by adopting a Bloch-sphere picture for the transition between $|0\rangle$ and $|1\rangle$ wherein the effects of spontaneous emission are to induce dephasing and relaxation of the state vector. For the 3-level system which describes

the $^{174}\text{Yb}^+$ ion, the picture is more complicated as decay to $|2\rangle$ leads to non-conservation of the probability current in the $\{|0\rangle, |1\rangle\}$ subspace. However, because we only care about the temporal evolution of $|1\rangle$, these effects can be ignored. The application of a time varying Rabi frequency drives the state vector from $|0\rangle$ to $|1\rangle$. Advancing the phase of $\Omega(t)$ by π can be thought of either as a virtual phase gate (i.e. a rotation about \hat{z}) or a reversal of the direction of motion of the state vector on the Bloch sphere. Thus, by controlling the relative rate and direction of rotation of the state vector, a solution can be found for any desired normalized profile of the excited state temporal distribution.

The inclusion of arbitrary phase in our system Hamiltonian leads to a quadratic increase in computational cost and introduces additional complexity for practical realization. Instead, recognizing parity control alone of phase is sufficient to coherently depopulate the excited state, we allow the driving field to take on negative Rabi frequencies in our simulation, corresponding to out-of-phase components of the laser. This allows efficient computation of the interaction Hamiltonian needed to produce photons of any temporal distribution. As expected, we find that as the emitter life time grows relative to a target photon's characteristic time scale, the ratio between the integral of in- and out-of-phase Rabi frequency components approaches 1, as shown in Fig. 4.

It should be noted that while only parity control of Rabi frequency phase is necessary to generate photons of any waveform for the case of resonant excitation, introduction of full phase modulation would allow deterministic photon waveform generation in the more general case of (known) time-dependent detuning.

III. QUANTUM MONTE CARLO TOOLS FOR PHOTON OPTIMIZATION

While the optimization methods described above allow the calculation of temporal distribution of photons emitted during a given excitation process, we cannot immediately extract information about the relative incidence of multi-photon emission events from $g(t)$ and $\langle N \rangle$ alone. Additionally, for multi-photon emission events, the temporal mode of each subsequently emitted photon will be distinct, as expected due to anti-bunching. The ability to characterize the distribution of each photon in such processes proves useful for implementing post selection to improve the performance of photon based networking protocols. Our approach to characterizing both emission statistics and waveforms in multi-photon events is to simulate many excitations and treat photon emissions as discrete quantum jumps. We then track the time and ordering of jumps (i.e. 1st photon emitted, 2nd photon emitted, etc.) for each trajectory.

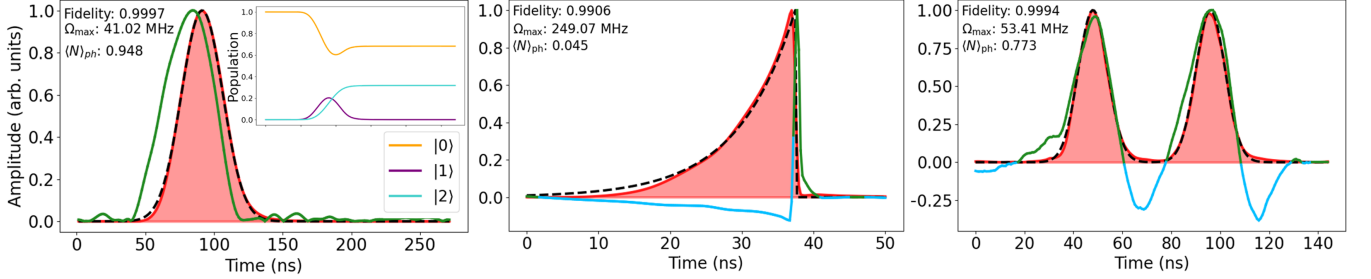


FIG. 3. Representative numerically predicted photon waveforms and optimized pulses. In all plots, green and blue solid lines represent in- and out-of-phase Rabi frequency relative amplitudes, dashed black lines show target photon distribution and filled red area shows predicted photon shape. **Left:** ‘Long’ photon demonstrating ability to produce waveforms with high fidelities, defined as the normalized mode overlap, and high $\langle N \rangle$ values without the use of phase modulation. Inset shows atomic populations during the excitation process. **Center:** An exponentially rising photon with $\tau_{\text{rise}} = 8.1$ ns, optimal for same qubit type state transfer. **Right:** Balanced double gaussian for time-bin atom-photon entanglement schemes.

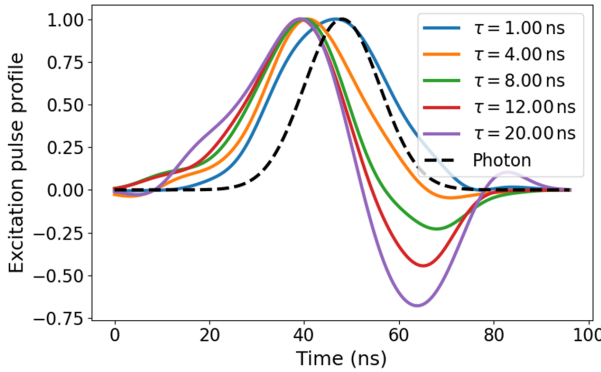


FIG. 4. Optimized excitation pulse shapes to produce a desired gaussian photon ($\sigma = 8$ ns) for emitters of a variety of lifetimes. As τ/σ grows, the corresponding pulse shape shows earlier phase flips and greater contribution of out-of-phase contributions to $\Omega(t)$.

A. Characterizing n-photon event emission statistics

Counting photon emission times and n -photon event ordering allows us to determine the prevalence of re-excitations for a desired photon waveform and mean emission number. Table I shows the photon emission statistics for various values of $\langle N \rangle$ matching Fig. 2. This approach can be used as a tool in the selection of appropriate excitation strengths when designing a particular photon generation protocol. For instance, for a general two-photon remote entanglement scheme, a typical merit function will involve both the photon generation rate from each node and the probability that a given photon came from an event with exactly one emission per node. As such, knowledge of relative emission probabilities proves valuable in setting experimental parameters.

$\langle N \rangle$	$P(0)$	$P(1)$	$P(2)$	$P(\geq 3)$
0.01	98.90%	1.10%	0.00%	0.00%
0.25	76.44%	22.96%	0.60%	0.00%
0.50	52.96%	44.08%	2.90%	0.06%
0.75	30.72%	63.32%	5.68%	0.28%
1.00	10.36%	80.02%	9.30%	0.32%

TABLE I. Emission statistics for various mean photon emission numbers $\langle N \rangle$. Columns $P(0)$, $P(1)$, $P(2)$, and $P(\geq 3)$ give the probability that a single excitation attempt produces 0, 1, 2, or more photons, respectively, corresponding to the waveforms shown in Fig. 2.

B. Multi photon temporal distributions and post selection

Additionally, we use trajectory statistics to bootstrap the temporal distribution of any photon (i.e. 1st, 2nd, etc.) sampled from trajectories when exactly n photons were emitted. We see that by examining the aggregate distribution of all jumps, we recover an average photon temporal profile that matches what we predict using the master-equation-only approach. For trajectories corresponding to the emission of a single photon, this distribution once again follows the master equation model for predicting $g(t)$. For higher order events where two or more photons are produced during a single excitation, the temporal distribution of photons shows the expected anti-bunching.

We can expand this approach to identify times after which any photon detected has a probability greater than a desired threshold to have been produced during a multi-photon emission event. This proves useful in improving post-selection of shots for entanglement generation protocols. Consider the case of a 1-photon remote entanglement scheme where we want to impose a constraint

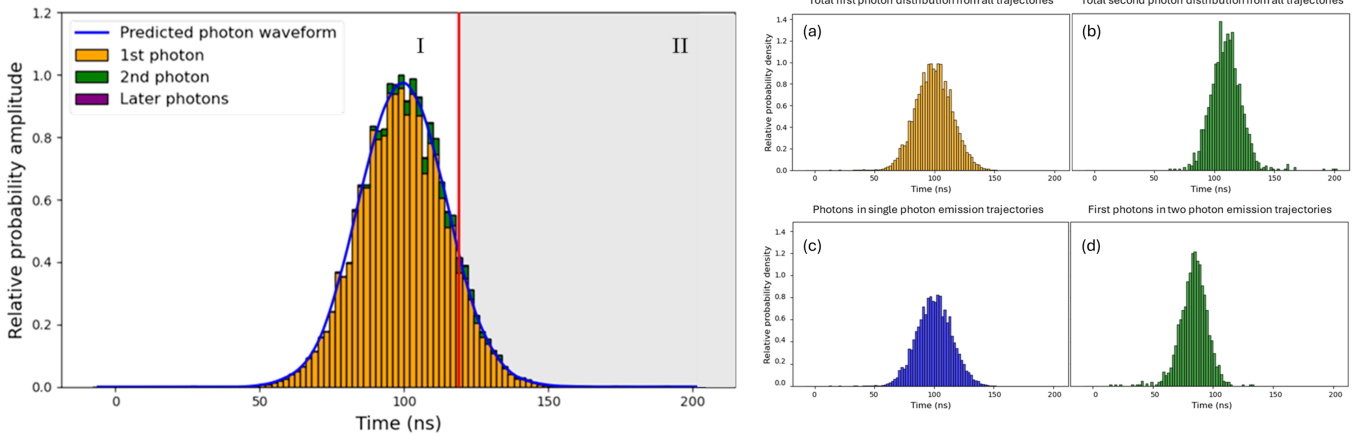


FIG. 5. Left: Illustration of time-of-detection based post-selection. The histogram shows simulated click-time densities for single-photon shots ($p_1(t)$, orange) and multi-photon shots ($p_2(t)$, green; $p_{\geq 3}(t)$, purple), normalized to unit area over clicks. The blue line shows the expected temporal distribution for the same process based on solution of the system master equation. The vertical red line marks a threshold for shots where the probability that a photon detection came from a multi-photon emission event is greater than 0.10, $P_{N \geq 2} = 0.10$. This is used to establish a cut time t^* . Accepting only shots in region I (i.e. $t \leq t^*$) raises the fraction of true single-photon heralds while reducing the acceptance rate. **Right:** Comparison of photon distributions for one and two photon emission events for the same excitation process. (a) normalized distribution of all first photon time-of-arrivals; (b) normalized distribution of all second photon time of arrivals; (c) normalized distribution of all first photon time of arrivals conditioned on the emission of only one photon; (d) normalized distribution of all first photon time of arrivals conditioned on the emission of two photons. We observe expected behavior for single and multi-photon events including: photon anti-bunching (see by comparing top right and bottom right panes) and a tighter, earlier distribution of first photons generated during two-photon emission trajectories vis-à-vis those coming from single-photon events.

that if a photon is detected, the probability that it came from a single emission event is greater than 0.90. Prior, the best we could do was to calculate the corresponding ratio of multi-photon events for a given $\langle N \rangle$. However, we have more information available to us than just this ratio. The intuition for our approach is straightforward. For our Λ system with excitation from $|0\rangle$ to $|1\rangle$, if a π photon is detected at a very early time in the excitation period, we expect the probability that this came from a multi-emission event to be much lower than if we detect the π photon very late in the pulse duration. Now, using trajectory data, we can quantify that intuition by looking at the ratio of n -photon events across the entire range of time bins. We can find the time after which a photon that is detected is more than 10% likely to be drawn from a multi-photon emission event and throw out all shots where the time of detection is after this cutoff. Fig. 5 illustrates this concept.

One subtlety to note here is that the act of throwing out certain counts changes the temporal distribution of photons detected during ‘good’ times. The associated temporal waveform for the set of post-selected photons will be given by the ensemble average of trajectories which satisfy the time-of-arrival condition. As such, care must be taken to ensure the conditioned temporal waveform from both nodes remains identical. For same-qubit-type systems this is trivially achieved by applying symmetric thresholds. However, for hybrid systems, this requires distinct thresholds to ensure the resultant dis-

tributions continue to match.

IV. TEMPORAL WAVEFORM CONTROL DEMONSTRATED WITH A TRAPPED ION

We demonstrate temporal photon waveform shaping in a trapped $^{174}\text{Yb}^+$ ion. A diagram of the apparatus for this experiment is shown in Fig. 6.

To implement photon shaping, alternating left (driving σ^- transitions) and right (driving σ^+ transitions) circularly polarized light is used to first optically pump to the $|0\rangle$ state and then drive an excitation to $|1\rangle$ with an arbitrary Rabi frequency. We tightly focus each beam through an acousto-optical modulator (AOM) that is driven by a variable amplitude and phase RF waveform supplied by an AWG in order to apply the desired excitation pulse. The AWG is controlled by computer via a graphical user interface (GUI) we developed to run the experiment.

As ion motion during a trap period will lead to a phase dependent instantaneous Doppler shift in the ion frame, we synchronize the experimental duty cycle to the trap. This is done by triggering the pulse shaping AWG using the trap RF source.

In order to select a single polarization to reconstruct the photon temporal waveform, π decay is mapped to a linear lab-frame representation and a Glan-Thompson polarizer is added to the collection optics directly before

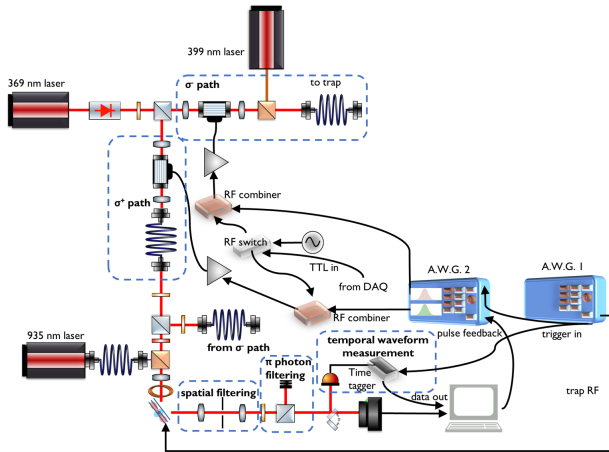


FIG. 6. Experimental apparatus for photon waveform control in a trapped $^{174}\text{Yb}^+$ ion system. An AWG sends RF waveforms to two AOMs. The AOMs pulse shape tightly focused, high polarization purity laser beams to implement optical pumping and pulsed excitation. Pulses are applied to an ion located in a 4-rod RF trap. A 0.41 numerical aperture objective is used to collect photons emitted from the ion. Photons are filtered to select only π decay. Time of arrival of photons is detected with a photon multiplier tube and high resolution time tagger. Both the time tagger and AWG are synchronized to the trap RF drive. The photon waveform is reconstructed over many shots.

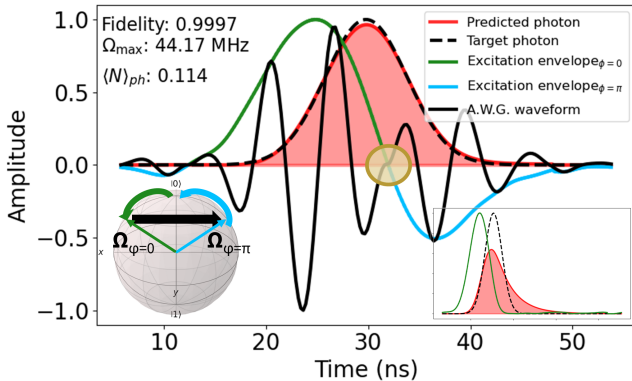


FIG. 7. The predicted excitation pulse needed to produce a short photon showing the corresponding RF waveform generated by the AWG. The highlighted gold region indicates how an optical π phase change is realized by advancing the RF by half a period for negative Rabi frequencies. The lower left inset shows the conceptual Bloch sphere picture illustrating how modulation of laser phase drives coherent de-excitation. The lower right inset shows the best pulse shape and photon possible with amplitude modulation only.

the photon multiplier tube (PMT) used to detect emissions. Photon histograms are assembled by sending the output of the PMT to a fast time resolving pulse counter (the time tagger), also triggered by the trap RF source.

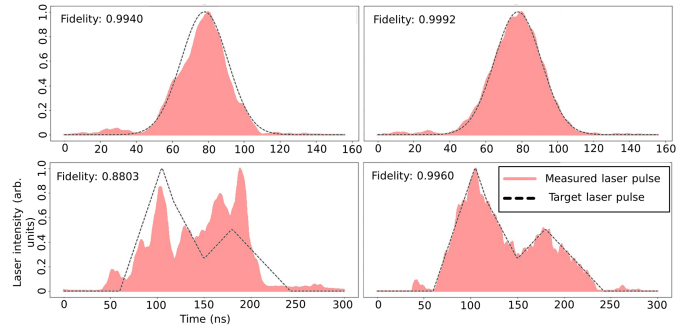


FIG. 8. Experimentally measured laser pulse shapes for smooth (top) and discontinuous (bottom) target pulses. Left panels show initial pulse shape, generated by applying the desired waveform as envelope to the RF signal sent to the AOM. Mismatch between target (dashed black line) and generated pulse arises due to a variety of experimental error sources including finite AWG bandwidth, impedance mismatch between various circuit elements and optical interference. Right panels show measured pulse after optimization.

A. Excitation pulse synthesis

To generate temporally shaped pulses, we must be able to modulate the amplitude of the 369 nm laser at speeds comparable to the characteristic time scale of the atomic response, determined by the 8 ns lifetime. Based on the acoustic wave velocity in our 130 MHz AOMs, this requires focusing the lasers down to ≈ 10 microns in the AOM crystal. The AWG provides an RF waveform which controls the amplitude and phase of the resultant optical pulse. A conceptual representation of RF waveform construction for a short target photon is shown in Fig. 7. Due to electronic bandwidth limits, finite AOM shuttering speeds and nonlinear effects in both the RF chain and acoustic wave excitation in the AOM, the optical pulse does not perfectly follow the AWG waveform.

To reduce infidelity in photon shaping resulting from errors in pulse synthesis, we employ the same optimization algorithms developed for numerical prediction of target laser pulse profiles to generate a given photon. By adjusting the inputs and outputs of these algorithms to communicate with experimental hardware, we can use the same approach to measure laser pulses and update AWG waveforms until suitably high fidelity excitation pulses are synthesized. This is done by detecting the time of arrival of photons from an attenuated pulse using the PMT/time tagger setup with the time tagger detection window synchronized to the start of the pulse. We can thus reconstruct the laser pulse amplitude and feedback on the RF waveform to perform optimization. This approach allows for the preparation of excitation pulses whose relative amplitudes match the desired pulse shape with fidelities, defined by the cosine similarity between measured and target pulses, of between 0.995 and 0.999 for distributions longer than ≈ 40 ns depending on the particular form of the desired pulse. Below this

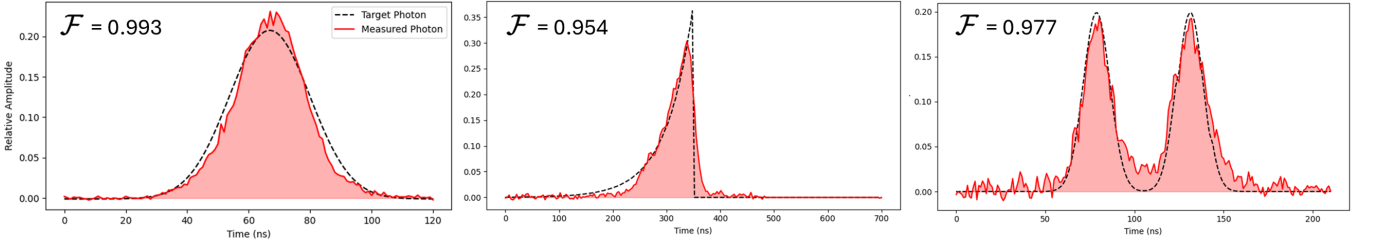


FIG. 9. Experimentally measured photon waveforms for three representative distributions. Photon histograms were constructed via repeated optical pumping and pulsed excitation sequences with photon time of detection synchronized to laser pulse triggers. Ion scatter is collected for several minutes to generate raw data. A background signal is then measured while the ion is pumped into a dark state. Histograms are constructed using this background-subtracted signal which accounts for the apparent negative amplitudes in some distributions owing to noise.

time scale, hardware limits the production of high fidelity pulses.

While our pulse synthesis approach yields high quality optical pulse amplitudes, we realize the optical phase changes needed to drive coherent de-excitation by changing the RF phase of the AOM wave, supplied by the AWG. Without a homodyne measurement apparatus, we cannot directly verify the phase relationship between different points in a single optical pulse. As such, we first optimize the laser pulse amplitude to match the desired form, and then apply the needed RF phase changes to the final AWG waveform.

B. Results

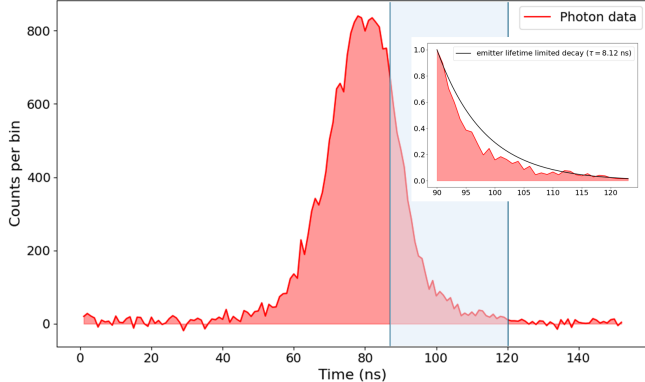


FIG. 10. Measured photon data for a representative short photon. The inset shows the data in the area highlighted in light blue, between 90 and 120 ns, with the lifetime limited exponential decay overlaid on measured data. By modulating the phase of the excitation pulse, coherent de-excitation allows a decrease in relative photon amplitude at a rate faster than would otherwise be possible.

Results of single photon measurements show good agreement with target waveforms. For ions cooled close to the Doppler limit, we can readily achieve waveform fi-

delities of greater than 0.99. Several representative photon distributions are shown in Fig. 9. Additionally, we validate our phase modulation method by comparing the fastest decay observed in short photon waveforms with the case of excited state lifetime limited decay rates. Fig. 10 reflects one such distribution. We see experimental confirmation that distributions shorter than would be allowed by lifetime limited decay are possible. Due to the hardware limitations described in the previous section, we are only able to demonstrate photon distributions slightly shorter than the lifetime limit. However, with appropriately fast modulators and sufficiently short optical pulses, we expect that photons of any arbitrarily short distribution could be generated.

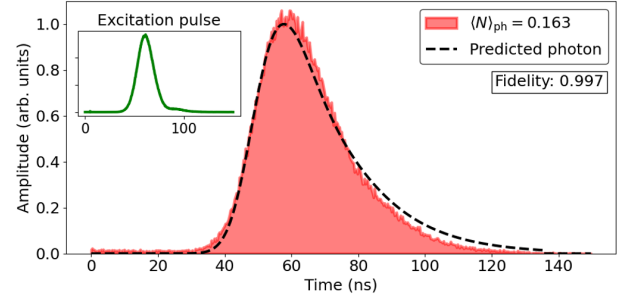


FIG. 11. Representative feedforward photon waveform verification. In order to estimate achievable single photon temporal shaping fidelities, we construct a photon histogram from a single ion without synchronization to the trap RF. By taking an aggregate of many initial relative phases between an ion undergoing micromotion and the excitation laser, the result approximates the equivalent photon shape expected when no micromotion is present. As such, we use this measurement to predict an achievable photon waveform preparation fidelity for a trap with fully compensable micromotion. We generated the predicted photon curve by feeding the measured excitation pulse (inset) into the system master equation. The red filled-in area denotes the measured photon histogram.

We attribute infidelity in photon waveforms to several sources including the previously mentioned limitations in optical pulse synthesis. However, we find that the error source of the greatest magnitude arises from non-

compensable micromotion in our ion trap which induces an RF phase dependent modulation of scattering rate. This unintentional scattering rate modulation is due to the fact that the ion essentially undergoes a range of instantaneous Doppler shifts over the course of a single excitation. The RF period for our trap is 93 ns and as such these effects are significant for any target photon distribution with characteristic time close to or greater than this value. As the shortest optical pulses we can synthesize are of the same order of magnitude, these effects are present in all measured distributions.

The micromotion present in our ion trap is a result of misalignment of the trap geometry during construction. The trap lacks adequate compensation electrodes to fully cancel the effects of this misalignment. As such, we expect that a system with higher tolerance manufacturing and sufficient compensation of stray fields would be capable of reducing the effects of micromotion in single photon shaping to negligible levels. To estimate achievable photon shaping fidelities in the absence of micromotion, we measure a photon histogram without synchronizing the excitation pulse or photon time of detection to the trap RF. This feedforward verification approach amounts to averaging out the micromotion so that the resultant histogram should reflect the ideal case where the ion undergoes no RF phase dependent Doppler shift. One such verification distribution is shown in Fig. 11. Therefore, it is important to note that the phase averaged distribution shown in Fig. 11 is not a true single photon estimate from our system, unlike the photon histograms shown in Fig. 9. However, based on the measured phase averaged histogram, we can estimate an achievable photon shaping fidelity of 0.996. We arrive at this estimate by measuring an applied laser pulse, predicting the expected photon distribution for this pulse and comparing to the phase averaged distribution.

V. CONCLUSION

We have demonstrated a conceptual and experimental method to generate photons of an arbitrary temporal waveform from single quantum emitters. Via the modulation of the amplitude and phase of a field which couples a ground state to a higher level undergoing radiative decay, we find that emitters of any lifetime can produce photons with any temporal distribution with restrictions in emission probability determined by intrinsic emitter properties. Numerical optimization methods can be used to arrive at the ideal form of the interaction Hamiltonian necessary to produce target photon shapes. Quantum Monte Carlo based tools can be used to characterize emission statistics and reconstruct conditional photon distributions for multi-emission events. These tools allow improved identification of appropriate pulse shapes

and strengths for quantum network protocols as well as shot post selection to increase fidelities for remote entanglement schemes. We tested photon temporal shaping for trapped $^{174}\text{Yb}^+$ ions and estimate achievable photon preparation fidelities of greater than 0.996. Experimentally, the photons we generate have lower temporal waveform fidelities than this estimate owing to the effects of non-compensable micromotion in our ion trap. Ultimately, the set of target waveforms which we can generate in our experimental apparatus are limited by minimum excitation times and feature resolution. In the future, we aim to improve experimentally demonstrated photon shaping by upgrading infrastructure to allow full compensation of ion micromotion and the generation of excitation pulses with higher temporal resolutions and shorter times.

ACKNOWLEDGMENTS

This work was supported by U.S. Department of Energy, Office of Science, Office of Basic Energy Sciences under Award No. DE-SC0020378.

Appendix A: Limits on $\langle N \rangle$ for a target temporal shape

We can derive an upper limit on an achievable value $\langle N \rangle$ for a target photon distribution, $g(t)$, by relating the target distribution to the limits of the excited state probability. We can write

$$P_1(t) = s \times g(t) \quad (\text{A1})$$

where s is a scaling parameter that enforces $P_1(t)_{\max} \leq 1$ where $P_1(t) \equiv \rho_{11}(t)$. To find an upper limit for $\langle N_q \rangle$, we set $s = 1/\max(g(t))$. This yields

$$\langle N_q \rangle_{\max} \leq \frac{\Gamma_q}{\max(g(t))} \int_{t_0}^{t_f} g(t) \left[1 - e^{-\Gamma(t_f - t)} \right] dt. \quad (\text{A2})$$

The bracketed term in the above inequality accounts for the fact that only a fraction of the population at some time, t , will contribute to photon emission by the completion of the pulse cycle at time t_f . The inequality arises due to the incoherent nature of spontaneous emission leading to a limit on the ability to deterministically populate (or depopulate) the excited state at any time, $t > t_0$. The amplitude of this effect relies heavily on the particular form of $g(t)$ and the characteristic dephasing time of a particular emitter with no general analytical form for any arbitrary distribution. However, emitters with relatively higher intrinsic dephasing time, T_2^* , and photon distributions with heavier weights at early times will more closely approach this limit.

-
- [1] S. Olmschenk, D. Hayes, D. N. Matsukevich, P. Maunz, D. L. Moehring, and C. Monroe, *International Journal of Quantum Information* **08**, 337 (2010).
- [2] J. F. Lilieholm, V. Niaouris, A. Kato, K.-M. C. Fu, and B. B. Blinov, *Applied Physics Letters* **117**, 154002 (2020), eprint: https://pubs.aip.org/aip/apl/article-pdf/doi/10.1063/5.0019892/14541946/154002_1.online.pdf.
- [3] Y. Chu, J. D. Pritchard, H. Wang, and M. Weides, *Applied Physics Letters* **118**, 240401 (2021), eprint: https://pubs.aip.org/aip/apl/article-pdf/doi/10.1063/5.0057740/14548794/240401_1.online.pdf.
- [4] H. K. Beukers, M. Pasini, H. Choi, D. Englund, R. Hanson, and J. Borregaard, *PRX Quantum* **5**, 010202 (2024).
- [5] J. D. Siversn, J. Hannegan, and Q. Quraishi, *Physical Review Applied* **11**, 014044 (2019).
- [6] S. Yu, K. Lee, S. Park, K. Kim, J. Goo, J. Park, and T. Kim, *Applied Physics Letters* **126**, 084001 (2025).
- [7] B. B. Blinov, D. L. Moehring, L.-M. Duan, and C. Monroe, *Nature* **428**, 153 (2004).
- [8] J. McKeever, A. Boca, A. D. Boozer, R. Miller, J. R. Buck, A. Kuzmich, and H. J. Kimble, *Science* **303**, 1992 (2004).
- [9] E. Knall, C. Knaut, R. Bekenstein, D. Assumpcao, P. Stroganov, W. Gong, Y. Huan, P.-J. Stas, B. Machielse, M. Chalupnik, D. Levonian, A. Suleymanzade, R. Riedinger, H. Park, M. Lončar, M. Bhaskar, and M. Lukin, *Physical Review Letters* **129**, 053603 (2022).
- [10] L. Stephenson, D. Nadlinger, B. Nichol, S. An, P. Drromta, T. Ballance, K. Thirumalai, J. Goodwin, D. Lucas, and C. Ballance, *Physical Review Letters* **124**, 110501 (2020).
- [11] K. Sosnova, *Mixed-Species Ion Chains for Quantum Networks*, Ph.D. thesis, University of Maryland, College Park.
- [12] T. Faorlin, B. Yadin, Y. Weiser, G. Araneda, S. Nimmrichter, L. Panzl, T. Lafenthaler, R. Blatt, T. Monz, and G. Cerchiari, *Controlling the spontaneous emission of trapped ions* (2025), version Number: 2.
- [13] L. Slodička, G. Hétet, N. Röck, P. Schindler, M. Henrich, and R. Blatt, *Physical Review Letters* **110**, 083603 (2013), publisher: American Physical Society.
- [14] S. L. N. Hermans, M. Pompili, L. D. Santos Martins, A. R-P Montblanch, H. K. C. Beukers, S. Baier, J. Borregaard, and R. Hanson, *New Journal of Physics* **25**, 013011 (2023).
- [15] L.-M. Duan, B. Blinov, D. Moehring, and C. Monroe, *Quantum Information and Computation* **4**, 165 (2004).
- [16] T. Van Leent, M. Bock, F. Fertig, R. Garthoff, S. Eppelt, Y. Zhou, P. Malik, M. Seubert, T. Bauer, W. Rosenfeld, W. Zhang, C. Becher, and H. Weinfurter, *Nature* **607**, 69 (2022).
- [17] H. Bernien, B. Hensen, W. Pfaff, G. Koolstra, M. S. Blok, L. Robledo, T. H. Taminiau, M. Markham, D. J. Twitchen, L. Childress, and R. Hanson, *Nature* **497**, 86 (2013).
- [18] V. Krutyanskiy, M. Galli, V. Krcmarsky, S. Baier, D. Fioretto, Y. Pu, A. Mazloom, P. Sekatski, M. Canteri, M. Teller, J. Schupp, J. Bate, M. Meraner, N. Sangouard, B. Lanyon, and T. Northup, *Physical Review Letters* **130**, 050803 (2023).
- [19] A. Craddock, J. Hannegan, D. Ornelas-Huerta, J. Siversn, A. Hachtel, E. Goldschmidt, J. Porto, Q. Quraishi, and S. Rolston, *Physical Review Letters* **123**, 213601 (2019).
- [20] M. Stobińska, G. Alber, and G. Leuchs, *EPL (Europhysics Letters)* **86**, 14007 (2009).
- [21] A. Golla, B. Chalopin, M. Bader, I. Harder, K. Mantel, R. Maiwald, N. Lindlein, M. Sondermann, and G. Leuchs, *The European Physical Journal D* **66**, 190 (2012).
- [22] J. I. Cirac, P. Zoller, H. J. Kimble, and H. Mabuchi, *Physical Review Letters* **78**, 3221 (1997).
- [23] S. Saha, M. Shalaev, J. O'Reilly, I. Goetting, G. Toh, A. Kalakuntla, Y. Yu, and C. Monroe, *Nature Communications* **16**, 2533 (2025).
- [24] P. Maunz, D. L. Moehring, S. Olmschenk, K. C. Younge, D. N. Matsukevich, and C. Monroe, *Nature Physics* **3**, 538 (2007), publisher: Nature Publishing Group.
- [25] P. P. Rohde, T. C. Ralph, and M. A. Nielsen, *Physical Review A* **72**, 052332 (2005), publisher: American Physical Society.
- [26] F. Sośnicki, M. Mikolajczyk, A. Golestanian, and M. Karpiński, *Nature Photonics* **17**, 761 (2023).
- [27] P. Kolchin, C. Belthangady, S. Du, G. Y. Yin, and S. E. Harris, *Physical Review Letters* **101**, 103601 (2008).
- [28] L. J. Wright, M. Karpiński, C. Söller, and B. J. Smith, *Physical Review Letters* **118**, 023601 (2017).
- [29] F. Sośnicki and M. Karpiński, *Optics Express* **26**, 31307 (2018).
- [30] R. L. Lecamwasam, M. R. Hush, M. R. James, and A. R. R. Carvalho, *Physical Review A* **95**, 013828 (2017).
- [31] M. Keller, B. Lange, K. Hayasaka, W. Lange, and H. Walther, *Nature* **431**, 1075 (2004).
- [32] X. You and Y.-M. He, *Physical Review Research* **7**, L012016 (2025).
- [33] J. P. Covey, H. Weinfurter, and H. Bernien, *npj Quantum Information* **9**, 90 (2023).
- [34] G. S. Vasilev, D. Ljunggren, and A. Kuhn, *New Journal of Physics* **12**, 063024 (2010).
- [35] A. Kuhn, M. Hennrich, and G. Rempe, *Physical Review Letters* **89**, 067901 (2002).
- [36] P. B. R. Nisbet-Jones, J. Dilley, A. Hollecze, O. Barter, and A. Kuhn, *New Journal of Physics* **15**, 053007 (2013).
- [37] D. L. Moehring, P. Maunz, S. Olmschenk, K. C. Younge, D. N. Matsukevich, L.-M. Duan, and C. Monroe, *Nature* **449**, 68 (2007).
- [38] C. Cabrillo, J. I. Cirac, P. García-Fernández, and P. Zoller, *Physical Review A* **59**, 1025 (1999).
- [39] J. Hofmann, M. Krug, N. Ortegel, L. Gérard, M. Weber, W. Rosenfeld, and H. Weinfurter, *Science* **337**, 72 (2012).
- [40] H. K. C. Beukers, M. Pasini, H. Choi, D. Englund, R. Hanson, and J. Borregaard [10.48550/ARXIV.2310.19878](https://arxiv.org/abs/2310.19878) (2023), publisher: arXiv Version Number: 1.
- [41] S. L. N. Hermans, M. Pompili, H. K. C. Beukers, S. Baier, J. Borregaard, and R. Hanson, *Nature* **605**, 663 (2022).
- [42] L. Luo, D. Hayes, T. A. Manning, D. N. Matsukevich, P. Maunz, S. Olmschenk, J. D. Sterk, and C. Monroe [10.48550/ARXIV.0906.1032](https://arxiv.org/abs/0906.1032) (2009), publisher: arXiv Version Number: 1.
- [43] D. N. Matsukevich, P. Maunz, D. L. Moehring, S. Olmschenk, and C. Monroe, *Physical Review Letters* **100**,

[150404 \(2008\).](#)